

Characteristics of sound radiation by turbulent flow over a hydrofoil and a bare-hull SUBOFF

Li Chen and Ian MacGillivray

Maritime Platform Division, Defence Science and Technology Organisation
506 Lorimer St, Fishermans Bend VIC 3207, Australia

ABSTRACT

In this study, the turbulent flows over a hydrofoil and the bare-hull SUBOFF are simulated using the unsteady/steady RANS model of FLUENT in order to show the distribution of noise sources. The sound radiation from hydrofoils with different spanwise dimensions and from SUBOFF is predicted for a model quadrupole source using the Boundary Element Method of SYSNOISE. It has been found that the scattered field for quadrupoles near the solid surface is mostly dipolar and that the scattering is more efficient when the sources are close to the edges. The trailing edge is a very efficient scatterer. The radiated field by the sources on the body of the hydrofoil and on the SUBOFF hull away from edges is mainly due to the radiation of the quadrupoles, and the scattering is very weak.

INTRODUCTION

Noise generated by turbulent flow has a critical impact on submarine stealth. Understanding of the characteristics of such noise therefore becomes important. Flow-induced noise sources from a complex structure such as a submarine may include noise from the rotation of the propeller, turbulence induced noise including scattered noise from the turbulent eddy passing a discontinuity of geometries (such as trailing-edge noise), cavity noise due to the interactions between turbulent flow and acoustic waves, and tonal noise induced by the coherent bluff-body-vortex shedding over appendages such as a sail, mast or control surface. The turbulence induced noises are mainly broadband in nature. There are three classes of prediction methods that can be used for the turbulence broadband noise: 1) a computationally expensive direct numerical simulation (DNS), 2) a semi-analytical solution and 3) a hybrid method (acoustic analogy combined with a computationally economic CFD). Application of the direct method to any practical problem is not feasible now and will be the case for some time to come. A semi-analytical method can be used very effectively in comparing different experiments and in design, and the absolute sound level can be only determined for some very simple models. A Hybrid method is able to predict the flow noise for arbitrary geometry and is feasible for the noise prediction of a complex geometry. However, the main obstacles faced by a Hybrid method are the expensive flow simulation and the requirement of some further modelling of the wave propagation. For a time-dependent solution of turbulent submarine flow, the required computational resources are very high, even without considering the numerical solution of wave propagation. Prediction of flow-induced noise by a full scale submarine or a structure of complex topology is only practically achievable using a Hybrid method, but still severely limited by currently available computational power.

The prediction of whole-submarine flow noise is challenging because it is a complex multi-physics problem. For example, turbulence noise radiation from a large smooth flat plate is broadband and of a quadrupole nature. Adding surface conditions complicates the noise generation mechanics. The

turbulence noise radiation from a trailing or leading edge is caused by the scattering of the broadband turbulence noise near the edge and is dipole in nature. Therefore, it would be very helpful to have a better understanding of the roles the hull body, sail and control surfaces play in the overall noise radiation as this will assist the management of the submarine stealth. The aim of this study is to contribute to this goal. However, in this report, only sound radiation due to a model quadrupole source is reported.

According to Lighthill (1952, 1954), the sound pressure, p , radiated by a turbulent flow has a quadrupole nature and is described by the inhomogeneous wave equation

$$\frac{\partial^2 p}{\partial t^2} - c^2 \frac{\partial^2 p}{\partial x_i^2} = \frac{\partial^2 T_{ij}}{\partial x_i \partial x_j} \quad (1)$$

The Lighthill stress tensor, T_{ij} , is given by

$$T_{ij} = \rho u_i u_j + (p - c^2 \rho) \delta_{ij} + \tau_{ij}, \quad (2)$$

where ρ , u , c , and τ are the fluid density, fluid flow speed, speed of sound, and shear stress tensor, respectively. An analytical solution of Eq. (1) can be found using a free space Green's function for some simple problems without solid surfaces, such as spinning vortex sound. However, to find an analytical solution of Eq. (1) for stationary or moving surfaces of arbitrary geometry is not trivial. Later, Ffowcs Williams and Hawkings (1969) developed the widely used FW-H model, based on Eq. (1), to account for the presence of surfaces which can be either stationary or moving relative to observers, based on a free space Green's function. The integral equation of the FW-H model is given with a penetrable surface equation as

$$Hc_0^2(\rho - \rho_0) = \frac{\partial^2}{\partial x_i \partial x_j} \int_V \frac{[T_{ij}]}{4\pi|\mathbf{x} - \mathbf{y}|} - \frac{\partial}{\partial x_i} \oint_S \frac{[p_{ij}]}{4\pi|\mathbf{x} - \mathbf{y}|} dS, \quad (3)$$

where ρ_0 and \mathbf{y} are the fluid density at far-field and source coordinate respectively. The volume integral is the

contribution of quadrupole sources and the surface integral may be considered as the contributions of monopole or dipole sources. The philosophy behind Eq. (3) is to locate a data surface $\zeta = 0$ around a moving noise-generating surface in such a way that most or all noise-producing quadrupoles are included within this surface so that no volume integration of the quadrupoles outside the data surface would be required. Theoretically, one must choose a penetrable data surface far away from the region where near-field flow is significant, and where the acoustic wave is propagating linearly, to avoid the cancellation between the surface integral and volume integral (Casper *et al.* 2004). Di Francescantonio (1997) and Casper and Farassat (2003) combined Kirchhoff's theory with the FW-H formula and proposed a boundary integral form of the FW-H penetrable surface equation, the so-called Formula 1B. They used it to predict trailing-edge noise. Kim *et al.* (2006) studied noise generated by flow over a hump using DNS and confirmed that Lighthill's source term in Eq. (1) correlated very well with the surface pressure fluctuation. Gloerfelt (2010) reached a similar conclusion from their Large Eddy Simulation (LES) simulation of turbulence boundary layer flows. The implication of those studies is significant, providing a very good foundation to combine a solver for Eq. (3) with a CFD simulation, which can provide the details of pressure history on the surface with an affordable computational cost. However, the ability of this method to account for the scattering of sound from non-compact surfaces depends on how the pressure p is defined.

For a non-compact and complex geometry, the solution of Eq. (1) could be obtained if exact Green's function and flow fields were specified. However, this is not normally trivial. Gloerfelt *et al.* (2005) developed a tailored Green's function for Eq. (1) to study the noise radiated by a cylinder in a cross flow and concluded that the surface integral obtained from Eq. (3) is the consequence of quadrupole scattering rather than due to a real physical source. As it may be expected that finding a tailored Green's function for Eq. (1) analytically for arbitrary geometries will be difficult, a numerical approach is the only choice. Therefore, a hybrid method of CFD and a boundary-element based wave equation solver (such as SYSNOISE) could be used to study the flow-induced sound for a complex geometry where the noise source is provided by CFD and the associated sound field is solved by FEM/BEM. However, as stated earlier, the aim of this study is to explore the radiation characteristics of a structure of complex geometry where simple primary quadrupole sources are used.

FLOW FIELD AND ASSOCIATED SOURCES

Turbulent flows over a hydrofoil of a large span are 2D dominant and have been investigated in a great detail using the unsteady RANS model in FLUENT (Do, Chen & Tu 2010). The general flow behaviour is shown in Figure 1a. A blunt trailing edge produces an energized vortex street with a distinctive frequency, and the boundary layer over the foil is fully turbulent over the majority of the surface for the given chord-length-based Reynolds numbers studied. The contours of turbulent kinetic energy and RMS-pressure fluctuations are highly concentrated around the aft region (Figure 1b), which indicates the location of the Lighthill tensor, and this is confirmed by DNS data of Sandberg and Sandham (2008).

The shape of the bare-hull version of the SUBOFF model is given in Figure 2. SUBOFF is a generic shape used for underwater flow studies (Liu & Huang 1998). Flow over this body was simulated using the $k \sim \omega$ turbulence model at

Reynolds number (Re) equal to 2.68×10^6 based on the length of the model. The distribution of turbulent kinetic energy and the typical turbulence length scale, which contributes to noise generation, is shown in Figure 3. The turbulent boundary layer is thin along the body and no separation is observed. At the aft end, the boundary layer expands significantly due to the curvature of the wall, where the flow becomes highly turbulent. The typical turbulence length scale based on turbulence kinetic energy k and turbulence dissipation rate ω is shown in Figure 3b, and is less than a millimetre, which is very small compared with the dimension of the model used for the flow simulation, of length 4.356 m and maximum radius 0.254 m. The total turbulence noise source due to mean shear-turbulence interaction and turbulence-turbulence interaction based on Lilley's method is estimated using FLUENT and is also illustrated in Figure 3. The self-noise source is due to the turbulence-turbulence interactions. It can be seen that the interactions between the turbulence and mean shear are the main contributors to the total source, which is highly concentrated at the aft end.

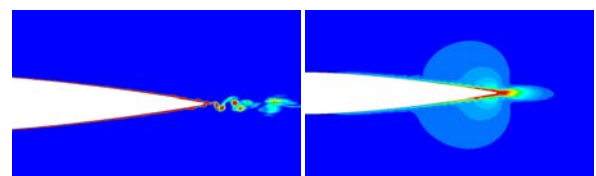


Figure 1. Flow field for a 2D foil at $Re = 2.68 \times 10^6$: (a) instantaneous vorticity magnitude contours ($0 \sim 600 \text{ s}^{-1}$); (b) contours of pressure fluctuation (RMS) ($100 \sim 1000 \text{ Pa}$).

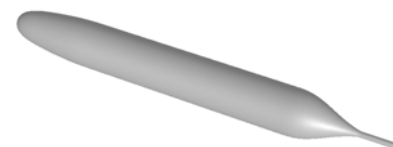


Figure 2. The schematic bare-hull SUBOFF model.

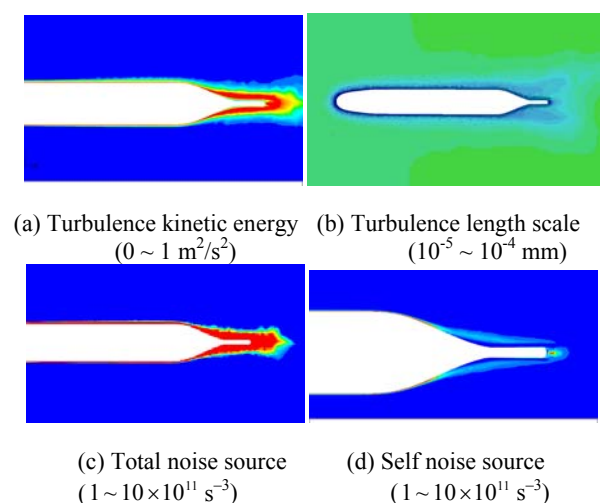


Figure 3. Turbulence and associated sound source distributions for the SUBOFF model at $Re = 2.68 \times 10^6$.

SOUND RADIATION FROM WALL-BOUNDED TURBULENT FLOW

According to Grighton *et al.* (1992), unsteady turbulent flows are acoustically equivalent to a particular quadrupole distribution radiating into a uniform acoustic medium. That is, the turbulent flow is comprised of many eddies, and each eddy has random phase relative to any other eddy. Inside each eddy the motion is well correlated, but uncorrelated with the motion inside other eddies. To get the sound field generated by a single eddy, one needs to add the density fields generated by points within the eddy, for they are all in-phase. To get the total intensity, one can sum the intensities from all separated eddies. For the generation of flow noise, the fine-scale structure of turbulence is largely irrelevant and only one length parameter is needed, representing the scale on which the turbulent energy is mainly concentrated. The flow simulations reveal that the turbulence induced source is compact over a wide range of frequency. Therefore, it is very useful to study the characteristics of radiated turbulence noise from a moving underwater structure using a model source.

A compact source scattering from a compact surface can be solved analytically with a high fidelity. However, with low Mach number and high Reynolds number flow as found in many underwater applications, the sources are compact but the structures are not. For instance, with the flow over the bare-hull SUBOFF, the overall turbulence length scales (l) are less than 1 mm, as shown in Figure 3b, much shorter than the corresponding acoustic wavelengths considered. The sources are therefore compact, but the model of length 4 m is not compact in terms of the acoustic wavelength associated with the turbulence flow frequency, u/l . The interaction between the surface and acoustic wave becomes complicated, and can be destructive or constructive. For such cases, there is no general solution, and a numerical approach provides the only practical solution, except for some special situations such as a semi-infinite plate. In this study we explore such interactions for underwater applications.

Lighthill's flow noise tensor, T_{ij} in the source term of Eq. (1), has a quadrupole nature. Since there are three components in each direction, nine possible independent orientations of the quadrupole axes exist. The orientation of the quadrupole source can be characterised as two classes —

longitudinal (+--+) and lateral $\begin{pmatrix} + & - \\ - & + \end{pmatrix}$. The diagonal

components of the Lighthill tensor have the three longitudinal orientations and the off-diagonal components have six lateral orientations. The contribution of the Lighthill tensor to turbulence boundary flow noise has been studied by Gloerfelt (2010), who confirmed the close relationship between the overall sound level and the surface pressure fluctuation using LES. According to Chase (1987), the wall pressure fluctuation beneath the turbulence boundary layer is proportional to the mean shear and the normal stress. To explore the contribution of the T_{ij} to the wall pressure spectra is beyond the scope of this report and will be addressed in a future study. However, for a homogenous turbulence flow with the absence of a solid surface, the far-field sound would be governed mainly by radiation of lateral quadrupole sources, with intensity changing as M^5 . In the presence of a surface, the radiation of the combined lateral and longitudinal quadrupole sources will be enhanced, with

the enhancement determined by the geometry of the surface. According to Blake (1986), Chase (1987), Grighton *et al.* (1992), and Wang & Moin (2000), for turbulent boundary layer flows with a geometrical discontinuity, the contribution of the Lighthill tensor to the scattering may be mainly due to the quadrupole having two axes normal to the surface. In this study, the radiation by T_{21} (lateral quadrupole) and T_{22} (longitudinal quadrupole) are investigated, where $i = 1$ is the streamwise direction and $i = 2$ is the vertical direction. These two quadrupoles satisfy the above condition and are the main contributors to the total Lighthill tensor responsible for the generation of turbulent boundary layer flow noise (Kim *et al.* 2006). It is worth emphasizing that it is not the intention of this study to replicate realistic turbulence noise sources.

The sound radiated by a hydrofoil (in 2D and 3D) and SUBOFF are studied using both line and point lateral/longitudinal quadrupole sources of unit strength located at different locations using SYSNOISE. They are the main contributors to the total Lighthill tensor responsible for the generation of the turbulent boundary layer flow noise (Kim *et al.* 2006). The inhomogeneous wave equation, Eq. (1), is solved by SYSNOISE. For this acoustic analysis the models were scaled down to length 0.335 m, with a maximum diameter 0.04 m, and an aft extension rod shorter than shown in Figure 3. The simulations were carried out with a variety of surface meshes depending on the location of the acoustic sources. Mesh density was increased on the surface near each source, with a typical total element number of 1500 to 3000 for the SUBOFF shape and 4000 to 6000 elements for the 3D hydrofoil. The 2D hydrofoil used 280 elements. Increased resolution was used to check the accuracy of the calculation.

Sound Radiation by a lateral quadrupole near a 2D hydrofoil

The radiation character of vortex-shedding-induced noise from a hydrofoil can be best represented by using the model source near the surface. The sound radiated from a 2D hydrofoil of the same cross-sectional profile as the SUBOFF hull is simulated using a lateral quadrupole. As a schematic description, positions where the quadrupole sources are located along the models are shown in Figure 4. A lateral quadrupole line source representing a shear stress is located at the front (location A), 2 mm away from the leading edge, representing incoming turbulence, while sources at locations B (0.15 m downstream from the leading edge), C (0.26 m), D (0.301 m), E (0.323 m) and F (0.337 m), located slightly away from the surface at the same 2 mm distance, represent turbulent boundary layer induced sources.

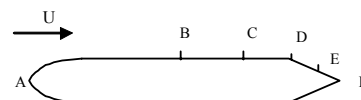


Figure 4. Locations of quadrupole sources.

The sound levels produced at 100 m distance from the foil by a model lateral quadrupole are given in Figure 5, and the near-field distribution of sound is shown in Figure 6. All dB values in this study are referenced to unit T_{ij} , equivalent to a reference 1 Pa if T_{ij} is 1 Pa. Note also that when scattering is dominant the total field is indistinguishable from the scattered field since the total is the sum of the scattered and

incident fields. It can be seen from Figure 5a for the lateral quadrupole source located at the aft that at a low frequency of 100 Hz ($L/\lambda = 0.02233$, where λ and L are the sound wave and the chord lengths respectively), the radiated sound pressure has the perfect dipolar directivity, $\sin(\theta)$, of a foil of a compact chord. Little sound radiates in the stream-wise directions and the peak sound pressure occurs in the direction normal to the surface of the foil. The total sound pressure is dominated by scattering and is 160 dB stronger than the incident. The radiation of sound is due to scattering from the trailing edge, and without the solid surface the radiation of the lateral quadrupole source is very weak.

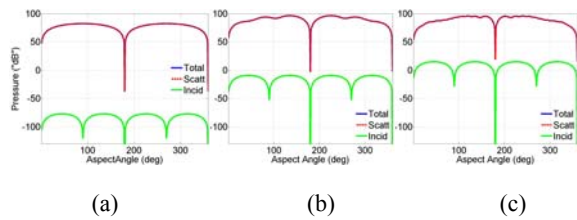


Figure 5. The incident, scattered and total sound pressure for a lateral quadrupole source near the aft of the 2D foil (Location F) for $f = 100, 5000, 20000$ Hz.

With an increase in frequency to 5 kHz, shown in Figure 5b, the chord length is now comparable to the wavelength ($L/\lambda = 1.1$). The distance between the source and trailing edge has increased slightly in terms of the acoustic wavelength, and the directivity of the sound pressure differs from 100 Hz due to the interactions between the wave diffracted by the leading edge and the reflected wave from the trailing edge. The directivity departs from $\sin(\theta)$, the compact dipole pattern, and shows extra ripples. The peak acoustic pressure is shifted towards the leading edge (0° is the downstream direction). The total radiated sound is still due to scattering but, is not as strong as for the lower frequency, being a 100 dB increase on the incident sound pressure. With a further increase in the frequency to 20 kHz (see Figure 5c), the chord is much larger than the wavelength ($L/\lambda = 4.5$) and the source is effectively further away from the surface. The directivity pattern is similar at 5 kHz. The relative scattering becomes weaker (although the absolute scattered levels are not lower), leading to a 70 dB increase in the sound pressure.

The effect of different locations of the lateral quadrupole sources is illustrated in Figure 6. When the source is located upstream of the leading edge, which represents impinging turbulence, the radiation is dominated by the scattering of the leading edge. Dipolar directivity is observed, confirming the theory of Howe (1998). The total sound levels vary with source location relative to the edges, and the variation depends upon the frequency. In general, as the source shifts closer to the trailing edge the scattered field (relative to the incident) becomes stronger (see Figures 6b to 6e). At 100 Hz, the change of the source location results in a small variation of the far-field sound level because the change of location is small compared with the wavelength, except at the location near the trailing edge, such as F, where scattering is strongest (see the first column of Figure 6e). The wedge angle of the edge plays a role as well: the smaller the wedge angle, the higher the radiated sound levels (Figure 6a and 6e). For 5 kHz, the scattering is enhanced with the source moving close to the trailing edge, as illustrated in the second column of Figure 6. The directivity pattern is changed slightly for the reasons discussed above. With a further increase in frequency

to 20 kHz, the influence of the leading edge becomes stronger, leading to the formation of ripples in the directivity. It is interesting to note that with the lateral source shifting towards the trailing edge, the scattering from the trailing edge becomes so strong that an induced source is formed there and eventually they merge as one source with a larger region.

Sound Radiation by a longitudinal quadrupole near a 2D hydrofoil

With a longitudinal quadrupole source, the directivity of the radiated sound is dipolar in nature, as for the lateral quadrupole, except for locations A and F. In those two situations, the dipole directivity rotates 90° and the peak sound pressure is upstream (or downstream) of the hydrofoil; the radiation is enhanced but the scattering is not as strong as with the lateral source. Shifting the source closer to the trailing edge, the scattering becomes stronger and the directivity of the far-field is the dipolar field of a compact chord, with the peak sound level perpendicular to the surface (directivities are not shown). As with the lateral quadrupole source, the radiated sound is strongest when the longitudinal source is near and above the trailing edge. However, the source located in the near wake does not radiate strongly. The leading edge shows a similar influence on the directivity to the lateral quadrupole source, resulting in the formation of directivity ripples.

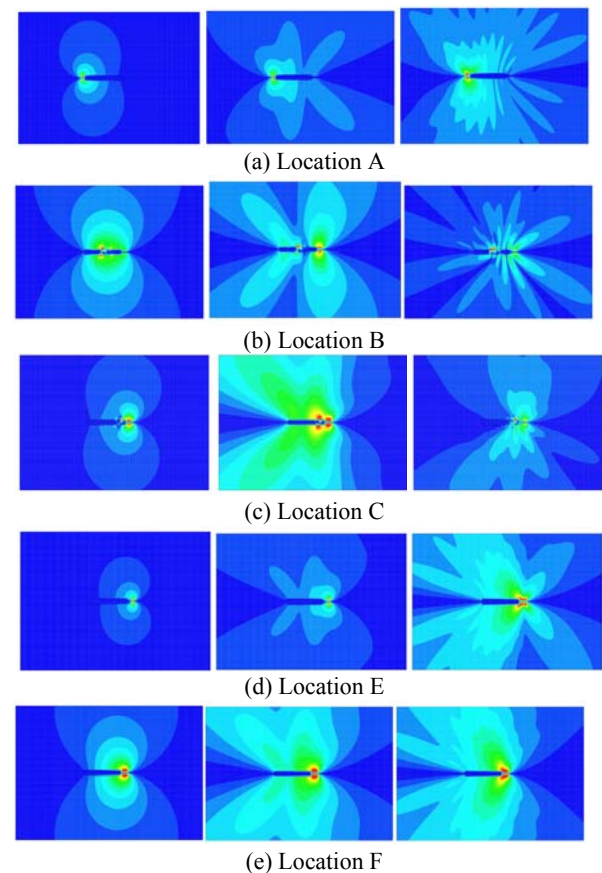


Figure 6. Scattered pressure for a lateral quadrupole source, using a fixed (but differing) linear pressure scale for each location: first column for 100 Hz, second column for 5 kHz and third column for 20 kHz.

The comparison of the difference between the total radiation and incident fields for the two quadrupoles is shown in Figure 7. It can be seen that the longitudinal quadrupole is the dominant contributor to the scattering when its axis is inline with the surface normal and radiates more efficiently when it is close to the trailing edge. This is consistent with the theory. This also reveals the mechanics of sound generation by a hydrofoil. Based on the CFD simulation of the hydrofoil at a small angle of attack (see Figure 1), the pressure fluctuation is strongest near the trailing edge. To reduce the noise generated by trailing edge flows, minimising the forcing on the trailing edge is important.

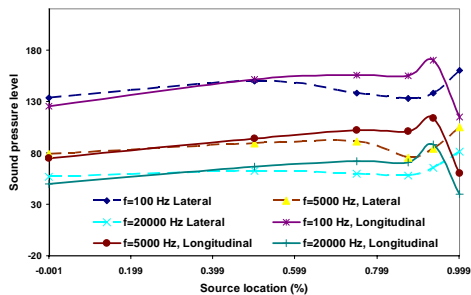


Figure 7. Comparison of the maximum increase in radiated sound pressure due to scattering by lateral and longitudinal quadrupole sources.

Sound Radiation by a lateral quadrupole near a 3D hydrofoil and SUBOFF

For many practical problems, there are no structures that are adequately represented by a 2D model of the real structure. It may be expected that the turbulence-noise scattering by a 3D structure would be different from a 2D structure. The sound radiated by a 3D hydrofoil with different spanwise dimension and the bare-hull SUBOFF have therefore been simulated using SYSNOISE. The 3D hydrofoil has the same profile as the 2D hydrofoil discussed above. Instead of extending to infinity in the spanwise direction, the 3D hydrofoil has a finite length. For each shape, a point quadrupole source with unit strength was used. This assumption approximates the turbulence quadrupole source in the real situation, which normally has a very small length scale.

The sound radiated by the 3D hydrofoil of a spanwise length 2 m with a source located at A (and centred on the spanwise dimension) for different frequencies is shown in the first column of Figure 8. The scattered field is indistinguishable from the total field in this figure. Compared with the 2D results, it can be seen that at a low frequency, the directivities for the two cases are very similar and are governed by $\sin(\theta)$. The scattering by the 3D foil is 50 dB stronger than the source for $f = 100$ Hz, but the far-field sound from a 2D foil is 160 dB stronger than the incident. Note that the levels for the 2D foil cannot be directly compared with the 3D foil due to the change in dimensionality. The influence of the leading edge is clearly identified, and the directivity is different from the 2D hydrofoil though it is a dipole field, in which the peak sound level shifts towards the trailing edge and the scattered wave becomes weak enough to produce a difference between the scattered and total sound levels. This difference increases with an increase in frequency (see Figures 8b and 8c). It is also noted that for the 3D hydrofoil the radiation is much weaker for all frequencies due to the nature of source and the shorter edge. For instance, at $f = 20$ kHz, the enhancement of the source is about 10 dB weaker than the 2D foil. At this frequency, the radiation is mainly due to reflection, doubling

the incident. Of course it is understandable that a 2D foil radiates more sound since it resembles the mechanics of noise induced by vortex shedding that is perfectly coherent in the spanwise direction.

Moving the source from location A to B, the radiated field is no longer consistently dipolar (first column in Figure 9). The directivity depends on frequency. For $f = 100$ Hz, the far field is dipolar and enhanced weakly due to scattering. With the frequency increased to 5 kHz, the scattering becomes destructive, leading to a quadrupole radiation weaker than the incident. A further increase in frequency to 20 kHz results in ripples that might be caused by scattering from the end of the finite span.

With the source at location F, the far field is dipolar and dominated by the scattering. It is enhanced by around 78 dB for $f = 100$ Hz (first column in Figure 10). With an increase in the frequency, the scattering become weaker and the presence of ripples in the directivity pattern reflects the influence of the leading edge and finite span. It can be seen that the trailing edge is a very efficient scatterer.

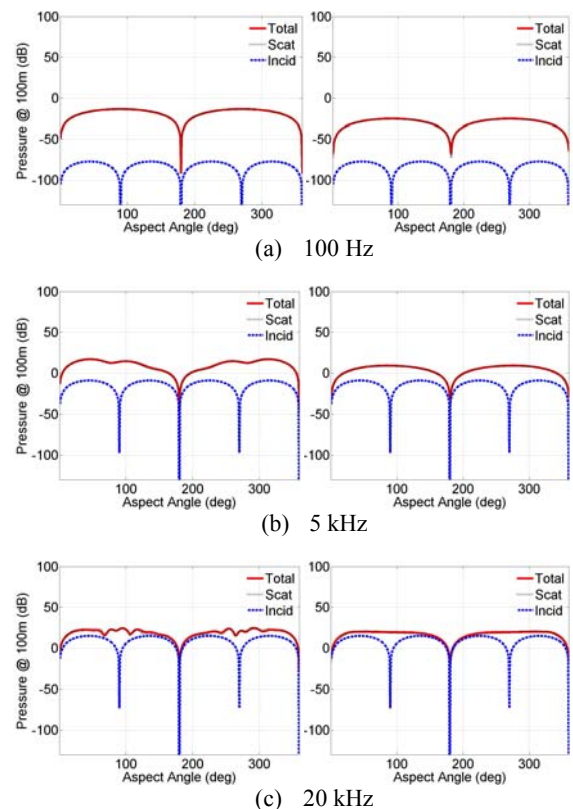


Figure 8. Radiation from the 3D hydrofoil and bare-hull SUBOFF at location A for different frequencies; first column for 3D hydrofoil of 2m span, second column for bare-hull SUBOFF.

The radiated sound fields from the bare-hull SUBOFF with a lateral quadrupole source located at different locations are illustrated in the second column of Figures 8, 9 and 10. At low frequency, it can be seen that the total sound is dominated by scattering with $\sin(\theta)$ dipolar directivity and peak sound pressure perpendicular to the hull surface. The radiation from the source at location A is enhanced the most due to its larger dimension in spanwise direction (second column in Figure 8). The enhancement of the incident field decreases with an increase in frequency.

The location of the source changes the directivity. For location B (Figure 9), the combination of the reflected and incident fields leads to cancellation. At a low frequency, dipolar directivity is maintained, and the radiation is dominated by the scattering. At $f = 5000$ Hz, the radiation is weaker than the incident but scattering is still largely dipolar and becomes destructive. With a frequency of 20 kHz, the radiation is the combination of incident and destructive reflection, leading to a quadrupole directivity. It can be seen that the lateral quadrupole sources located on the middle of SUBOFF would propagate with a very low efficiency.

The scattered field at location F (second column in Figure 10) is generally weaker than the incident, except at $f = 100$ Hz where SUBOFF is compact in all three dimensions. For $f = 5000$ Hz, the directivity of the radiation is due to the cancellation between the scattering and incident fields, though the scattering is dipolar with peak pressure perpendicular to the surface. At the highest frequency, 20 kHz, the scattering field is dipolar, but the radiation is dominated by the incident.

Unlike the scattering from a long trailing edge, the lateral quadrupole source located near the aft of SUBOFF radiates weakly.

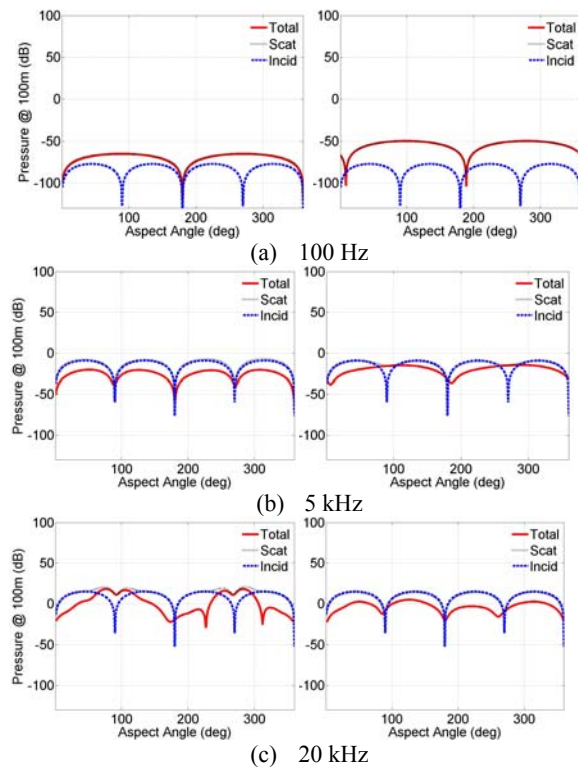


Figure 9. Radiation from the 3D hydrofoil and bare-hull SUBOFF at location B for different frequencies; first column for 3D hydrofoil of 2 m span, second column for bare-hull SUBOFF.

Comparison of the radiation by 3D hydrofoils of different spanwise dimensions and the bare-hull SUBOFF is illustrated in Figure 11.

For a hydrofoil of spanwise dimension of 0.5 m, the overall trend in the radiation directivity is similar to the hydrofoil of 2 m span. The far-field is amplified by a similar amount to the 2 m hydrofoil (Figure 11), because both geometries are acoustically compact. However, a stronger radiation field should be expected from a longer trailing edge due to the

larger “wetted” surface. When the source is close to an edge, the radiation is enhanced by scattering. The influence of the edges and finite span is clearly identified at 5 kHz by the presence of larger ripples than with the directivity of the 2 m hydrofoil. Like the 2 m hydrofoil, placing the sources midway along the chord results in a scattered field comparable to the incident but out of phase, leading to a radiation field weaker than the incident.

The incident field is enhanced significantly by the edges of 3D hydrofoil and the nose of SUBOFF due to scattering, which has dipolar directivity. The radiation from the hydrofoil increases with the increase in the span dimension in general. The trailing edge of the 3D hydrofoil behaves as a stronger scatterer. When the source is located in the middle, the SUBOFF model generally radiates more efficiently than the hydrofoils for all the frequencies (Figure 11b) with a dipolar directivity at 100 Hz and 5 kHz. The radiation field for the hydrofoil is quadrupole at 5 kHz and 20 kHz. However, in those cases, the scattering becomes destructive except at 100 Hz, leading to a radiation field weaker than the incident. At high frequencies, the spanwise dimension of the hydrofoil results in a significant change in the directivity.

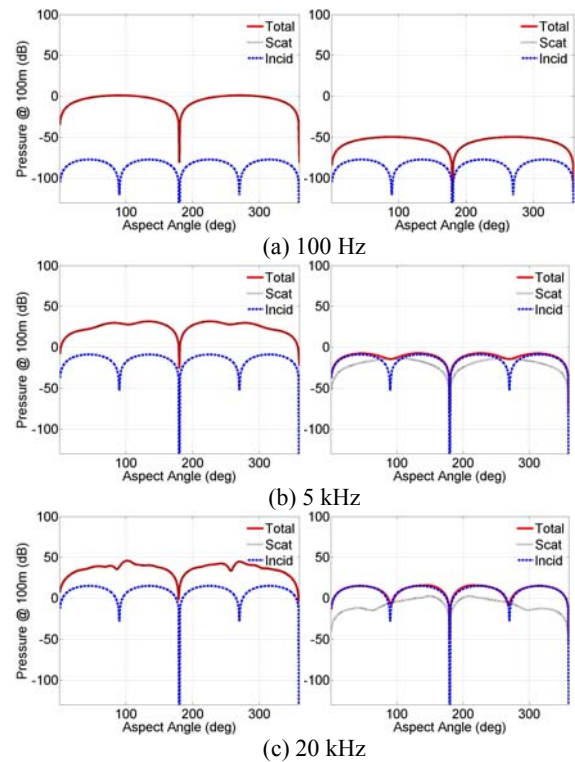


Figure 10. Radiation from the 3D hydrofoil and bare-hull SUBOFF at location F for different frequencies; first column for 3D hydrofoil of 2m span, second column for bare-hull SUBOFF.

Sound Radiation by a longitudinal quadrupole near a 3D hydrofoil and SUBOFF

The radiation of longitudinal quadrupoles, located at B and F, by the hydrofoil of 2 m span and the bare-hull SUBOFF, are depicted in Figures 12 and 13. Note that the radiation from the source at location A has a similar directivity to F and is not shown.

When a longitudinal quadrupole is applied at location B, the directivity is dipolar. The radiation from both the hydrofoil of 2 m span and the bare-hull SUBOFF show a similar

enhancement due to scattering at 100 Hz and 5 kHz (Figure 12). However, at a higher frequency of 20 kHz the scattering from the hydrofoil is stronger than that from SUBOFF, with a maximum sound pressure level perpendicular to the surface. Overall, the enhancement of the incident field for both the hydrofoil and SUBOFF decreases with an increase in frequency.

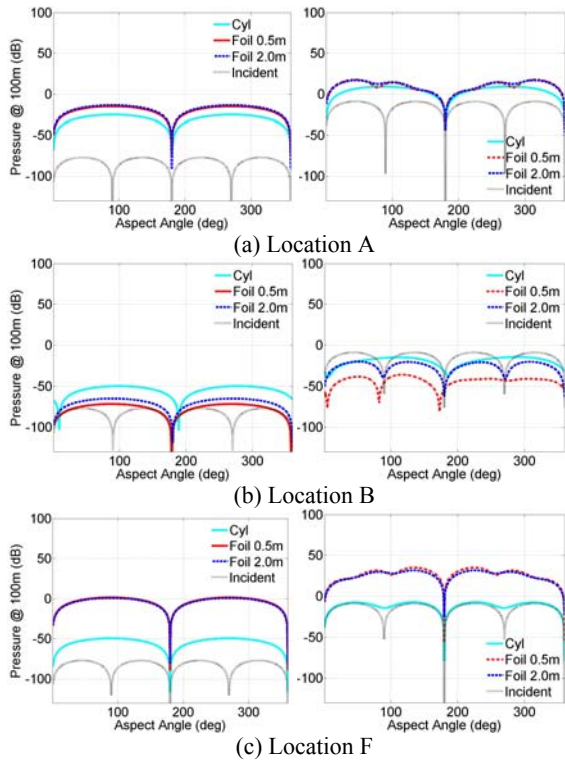


Figure 11. Comparison, between 3D structures, of radiated fields of a lateral quadrupole; first column for $f = 100$ Hz, second column for $f = 5000$ Hz.

Placing the source at locations F for 100 Hz leads to a dipolar radiation with a peak sound pressure at 0° and $\pm 180^\circ$ rather than at $\pm 90^\circ$. The radiation is also dominated by scattering. (See Figure 13a.). The enhancement of the incident field originating in the near wake of either the hydrofoil or SUBOFF is weaker compared with the radiation of a lateral quadrupole source. At higher frequencies, the directivity is different from the lateral quadrupole because of the nature of the source. The radiation field is nearly monopolar due to the combination of the incident and weak scattering fields (see Figures 13b and 13c). Like the lateral quadrupole, at a low frequency of 100 Hz the scattering of the incident field is dominant, but its destructive nature is clearly observed at higher frequencies, leading to a very weak radiation. For the hydrofoil, the source at the location F gives nearly monopolar radiation at higher frequencies, while for SUBOFF the scattered field is weaker than the incident field.

Overall, the radiation of the longitudinal quadrupole is enhanced by SUBOFF for low and middle frequencies, but only weakly. However, it is still stronger compared to the lateral quadrupole source, particularly for the source near the middle of SUBOFF. It can be seen that it is essential to have the details of the quadrupole source in order to predict the far field flow-induced noise.

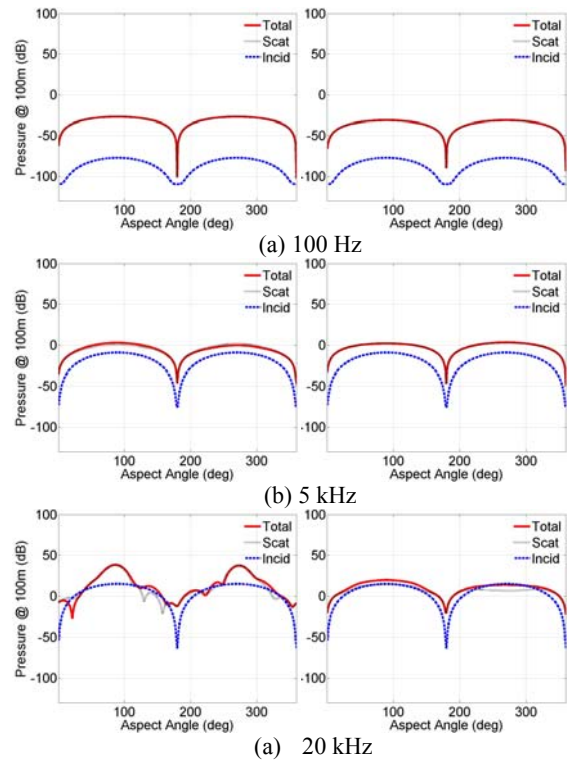


Figure 12. Directivity of a longitudinal quadrupole at location B at different frequencies for a 3D hydrofoil and the bare-hull SUBOFF.

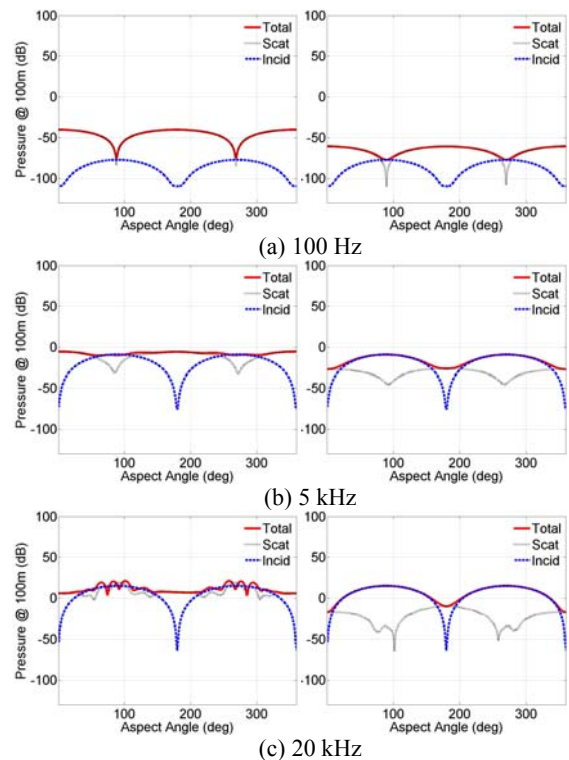


Figure 13. Directivity of a longitudinal quadrupole at location F for a 3D hydrofoil and the bare-hull SUBOFF.

CONCLUSION

A compact flow noise source near the trailing edge of the 2D and 3D hydrofoils is radiated efficiently due to the scattering mechanics and the spanwise extended nature of the foils. The directivities of the scattered fields over all frequencies are dipolar. Such scattering is strongly dependent upon the location and nature of the source and the topology of the structure and its dimension. For a general hydrofoil, sources with a strong coherence in the spanwise direction would be enhanced significantly. The edges of hydrofoils are responsible for the efficient scattering. A source reasonably far away from the edges does not radiate as strongly as those close to the edges. The directivity of the overall radiation field depends on the acoustic compactness of the hydrofoil. Those results imply that for a hydrofoil of a finite span the radiation of the turbulence-induced noise is mainly due to scattering at the edges.

For the SUBOFF model, a flow noise source near the nose will be enhanced efficiently and, with an increase in the distance from the nose, flow noise will be only enhanced weakly unless it is acoustically compact. The scattering from SUBOFF is dipolar, but the overall radiation field depends on the strength of the scattering. Sources located away from the nose radiate very weakly due to the cancellation between the scattering and incident fields. Only the nose of SUBOFF is an efficient scatterer compared with the other areas. At higher frequencies, the volume integral of Eq. (3) would be the main contributor to the total source.

It has been found that, in general, sources of a small scale located on the large surface of the 3D structures do not radiate efficiently. These results are consistent with the theory that the radiation of quadrupole high frequency turbulence over a large surface is not efficient.

Note also that the correlation length scale of the source is a critical parameter in term of the far field radiation. The main reason that the 2D hydrofoil scatters more efficiently is because it effectively uses a line source perfectly correlated in the spanwise direction. Our 3D hydrofoil used a point source centred on the span.

As a result of the above, it can be seen that any acoustic propagation model without a proper consideration of scattering will not be able to predict the low Mach flow-induced noise over an acoustically non-compact geometry.

REFERENCES

- Blake, WK 1986, *Mechanics of Flow-Induced Sound and Vibration*, Academic Press Inc. (London) Ltd.
- Casper, J & Farassat, F 2003, Broadband noise predictions for an Airfoil in a turbulent stream, AIAA 2003-0366.
- Casper, J, Lockard, DP, Khorrami, MR & Streett, CL 2004, Investigation of volumetric sources in airframe noise simulations, AIAA 2004-2805.
- Chase, D 1987, The character of the turbulent wall pressure spectrum at subconvective wavenumbers and a suggested comprehensive model, *Journal of Sound and Vibration*, vol. 112(1), pp. 127-147.
- Di Francescantonio, P 1997, A new boundary integral formulation for the prediction of sound radiation, *Journal of Sound and Vibration*, vol. 202(4), pp. 491-509.
- Do, T, Chen, L & Tu, JY 2010, Numerical study of turbulent trailing edge flows with base cavity effects using URANS, *Journal of Fluids and Structures*, vol. 26, pp. 1155-1173.
- Ffowcs Williams, JE & Hawkings, DJ 1969, Sound generation by turbulence and surfaces in arbitrary motion, *Phi. Trans. Roy. Soc.* A264, pp. 321-342.
- Gloerfelt, X, Pérot, F, Bailly, C & Juvé, D 2005, Flow-induced cylinder noise formulated as a diffraction problem for low Mach numbers, *Journal of Sound and Vibration*, vol. 287, pp. 129-151.
- Gloerfelt, X 2010, The link between wall pressure spectra and radiated sound from turbulent boundary layers, AIAA 2010-3904.
- Grington, DG, Dowling, AP, Ffowcs Williams, JE, Heckl, M & Leppington, FG 1992, *Modern Methods in Analytical Acoustics, Lecture notes*. Springer-Verlag.
- Howe, MS 1998, *Acoustics of Fluid-Structure Interactions*, Cambridge University Press.
- Kim, J & Sung, HJ 2006, Wall pressure fluctuations and flow-induced noise in a turbulent boundary layer over a bump, *J. Fluid Mech.* Vol. 558, pp. 79-102.
- Lighthill, MJ 1952, On sound generated aerodynamically, Part I: general theory, *Proc. Roy. Soc. Lond.* A211, pp. 564-587.
- Lighthill, MJ 1954, On sound generated aerodynamically, Part II: turbulence as a source of sound. *Proc. Roy. Soc. Lond.* A222, pp. 1-32.
- Liu, HL & Huang, TT 1998, Summary of DARPA Suboff experimental program data, CRDKNSWC/HD-1298-11, Naval Surface Warfare Center, Carderock Division.
- Sandberg, R & Sandham, N 2008, Direct numerical simulation of turbulent flow past a trailing edge and the associated noise generation, *Journal of Fluid Mechanics*, vol. 596, pp. 353-385.
- Wang, M & Moin, P 2000, Computation of trailing-edge flow and noise using Large-Eddy Simulation, *AIAA Journal*, vol. 38(12), pp. 2201-2209.